

Unusual tunability of multiferroicity in $GdMn_2O_5$ by electric field poling far above multiferroic ordering point

Xiang Li(李翔), Shuhan Zheng(郑书翰), Liman Tian(田礼漫), Rui Shi(石锐), Meifeng Liu(刘美风), Yunlong Xie(谢云龙), Lun Yang(杨伦), Nian Zhao(赵念), Lin Lin(林林), Zhibo Yan(颜志波), Xiuzhang Wang(王秀章), Junming Liu(刘俊明)

Citation: Chin. Phys. B . 2019, 28(2): 027502. **doi:** 10.1088/1674-1056/28/2/027502
Journal homepage: http://cpb.iphy.ac.cn; http://iopscience.iop.org/cpb

What follows is a list of articles you may be interested in

Voltage control of ferromagnetic resonance and spin waves

Xinger Zhao(赵星儿), Zhongqiang Hu(胡忠强), Qu Yang(杨曲), Bin Peng(彭斌), Ziyao Zhou(周子尧), Ming Liu(刘明)

Chin. Phys. B . 2018, 27(9): 097505. **doi:** 10.1088/1674-1056/27/9/097505

Magnetism manipulation in ferromagnetic/ferroelectric heterostructures by electric field induced strain

Xiaobin Guo(郭晓斌), Dong Li(李栋), Li Xi(席力)

Chin. Phys. B . 2018, 27(9): 097506. **doi:** 10.1088/1674-1056/27/9/097506

NMR evidence of charge fluctuations in multiferroic $CuBr_2$

Rui-Qi Wang(王瑞琦), Jia-Cheng Zheng(郑家成), Tao Chen(陈涛), Peng-Shuai Wang(王朋帅), Jin-Shan Zhang(张金珊), Yi Cui(崔祎), Chong Wang(王冲), Yuan Li(李源), Sheng Xu(徐胜), Feng Yuan(袁峰), Wei-Qiang Yu(于伟强)

Chin. Phys. B . 2018, 27(3): 037502. **doi:** 10.1088/1674-1056/27/3/037502

Lumped modeling with circuit elements for nonreciprocal magnetoelectric tunable band-pass filter

Xiao-Hong Li(李小红), Hao-Miao Zhou(周浩淼), Qiu-shi Zhang(张秋实), Wen-Wen Hu(胡文文)

Chin. Phys. B . 2016, 25(11): 117505. **doi:** 10.1088/1674-1056/25/11/117505

Magnetoelectric memory effect in the Y-type hexaferrite $BaSrZnMgFe_{12}O_{22}$

Fen Wang(王芬), Shi-Peng Shen(申世鹏), Young Sun(孙阳)

Chin. Phys. B . 2016, 25(8): 087503. **doi:** 10.1088/1674-1056/25/8/087503

Unusual tunability of multiferroicity in $GdMn_2O_5$ by electric field poling far above multiferroic ordering point*

Xiang Li(李翔)[1,2,†], Shuhan Zheng(郑书翰)[2], Liman Tian(田礼漫)[1], Rui Shi(石锐)[1], Meifeng Liu(刘美风)[1], Yunlong Xie(谢云龙)[1], Lun Yang(杨伦)[1], Nian Zhao(赵念)[1], Lin Lin(林林)[2], Zhibo Yan(颜志波)[2], Xiuzhang Wang(王秀章)[1], and Junming Liu(刘俊明)[1,2,3]

[1] *Institute for Advanced Materials, Hubei Normal University, Huangshi* 435002, *China*

[2] *Laboratory of Solid State Microstructures and Innovative Center of Advanced Microstructures, Nanjing University, Nanjing* 210093, *China*

[3] *Institute for Advanced Materials, South China Normal University, Guangzhou* 510006, *China*

(Received 6 September 2018; revised manuscript received 28 November 2018; published online 10 January 2019)

The multiferroicity in the $R Mn_2O_5$ family remains unclear, and less attention has been paid to its dependence on high-temperature (high-T) polarized configuration. Moreover, no consensus on the high-T space group symmetry has been reached so far. In view of this consideration, one may argue that the multiferroicity of $R Mn_2O_5$ in the low-T range depends on the poling sequence starting far above the multiferroic ordering temperature. In this work, we investigate in detail the variation of magnetically induced electric polarization in $GdMn_2O_5$ and its dependence on electric field poling routine in the high-T range. It is revealed that the multiferroicity does exhibit qualitatively different behaviors if the high-T poling routine changes, indicating the close correlation with the possible high-T polarized state. These emergent phenomena may be qualitatively explained by the co-existence of two low-T polarization components, a scenario that was proposed earlier. One is the component associated with the Mn^{3+}–Mn^{4+}–Mn^{3+} exchange striction that seems to be tightly clamped by the high-T polarized state, and the other is the component associated with the Gd^{3+}–Mn^{4+}–Gd^{3+} exchange striction that is free of the clamping. The present findings may offer a different scheme for the electric control of the multiferroicity in $R Mn_2O_5$.

Keywords: multiferroicity, $GdMn_2O_5$, high-T polarized state, exchange striction

PACS: 75.85.+t, 75.30.Kz, 77.80.–e **DOI:** 10.1088/1674-1056/28/2/027502

1. Introduction

The so-called type-II multiferroics, referring to the magnetically induced ferroelectricity, have enriched the connotation of condensed matter physics and materials science.[1,2] In these multiferroics, an electric polarization (P) emerges as a function of temperature (T) below the so-called multiferroic ordering temperature (T_{mo}), and is associated with a particular magnetic order and correlated with spin–orbital coupling or spin–phonon coupling.[3–6] In addition to interest from the point of view of fundamental research, these systems exhibit significant coupling between ferroelectricity and magnetism, offering potential for the magnetic control of ferroelectricity or electric control of magnetism.[7–9] Nevertheless, most of type-II multiferroics have low T_{mo}, relatively small P, and weak ferromagnetism. On the one hand, substantial efforts have been devoted to searching for additional multiferroics such as $CaMn_7O_{12}$ and $CaBaCo_4O_7$, which show giant improper ferroelectricity and gigantic magnetically induced polarization, respectively.[10–14] On the other hand, the underlying mechanisms and emergent phenomena in already available multiferroics have been investigated persistently.[15–17] Along this line, we discuss one class of type-II multiferroics, rare-earth manganite $R Mn_2O_5$ that has been considered due to its intriguing multiferroic mechanism and compelling physical properties.[18–20] It is our motivation that these unveiled mechanisms, if any, would be beneficial to our designing and synthesizing the novel materials with superior multiferroic properties.

The $R Mn_2O_5$ family, where R represents Y or rare earth ion, have complicated the physics of multiferroicity with large electric polarizations. It is noted that almost all members of the $R Mn_2O_5$ family have similar structures[21,22] as shown in Fig. 1(a), where $GdMn_2O_5$ is taken as an example. The Mn^{4+} and Mn^{3+} ions have different occupations with complicated symmetric and asymmetric exchange strictions and thus a strong spin frustration becomes inevitable.[23] With T decreasing, $R Mn_2O_5$ undergoes a magnetic transition from paramagnetism to incommensurate antiferromagnetic ordering at T_{N1}, followed by the transition to commensurate antiferromagnetic ordering at T_{N2} where a ferroelectric transition is identified.[24,25] This consistency indicates that the observed ferroelectricity in $R Mn_2O_5$ is magnetically induced, and thus

*Project supported by the National Natural Science Foundation of China (Grant Nos. 11804088, 11234005, 11374147, 51431006, and 11704109), the National Key Research Program of China (Grant No. 2016YFA0300101), and the Research Project of Hubei Provincial Department of Education, China (Grant No. B2018146).

†Corresponding author. E-mail: lixplus@126.com

© 2019 Chinese Physical Society and IOP Publishing Ltd

we have $T_{mo} \sim T_{N2}$. Here, an often misleading consequence associated with the intensive studies is that RMn$_2$O$_5$ should be paraelectric above T_{N2}.

The similarity in magnetic structure of RMn$_2$O$_5$ would imply the similarity of electric polarization in response to these magnetic ordering sequences in the low-T range. However, measured data from several systems[26–29] or even from the same system but different samples synthesized by different authors did show big scattering[18,30–32] as shown in Fig. S1 of Supplementary Material. This issue can be discussed more extensively from various aspects. First, when the general pyroelectric method is used, the measured pyroelectric current $I(T)$ and deduced polarization $P(T)$ as a function of T in the low-T range (< 50 K) are qualitatively different for different materials. In quite a few cases, different groups presented inconsistent data from the same system, which is quite unusual. Second, a two-polarization-component model in the low-T range is used to explain the observed phenomena in a recent topical review on ferroelectricity of RMn$_2$O$_5$.[33] In this model, the two components originating respectively from the symmetric R^{3+}–Mn^{4+}–R^{3+} and Mn^{3+}–Mn^{4+}–Mn^{3+} exchange strictions are available and they exhibit different T-dependence, contributing to the complicated overall $I(T)$ and $P(T)$ behaviors. This model does work well on DyMn$_2$O$_5$ and TmMn$_2$O$_5$ by describing the ferrielectric lattice but cannot be applied to other systems.[28,34,35] A major uncertainty is that the two polarization components may not necessarily be coupled with each other. Third, the mechanism for the magnetoelectric coupling is still not well understood yet, and inconsistent data about the change of magnetically induced polarization were reported from various groups in GdMn$_2$O$_5$.[30,31]

In addition, our preliminary measurements on DyMn$_2$O$_5$, GdMn$_2$O$_5$, YMn$_2$O$_5$, and TmMn$_2$O$_5$ revealed that the measured $I(T)$ and $P(T)$ data depend greatly on the detail of electrical poling of the samples in the high-T range ($\gg T_{N1}$).[28,35] The dependence brought us major difficulty in obtaining interconsistent data of the low-T multiferroicity. We may intentionally correlate the different electric poling sequences in the high-T range with different polarized states. For example, one defines a starting temperature T_{st} ($\gg T_{N1}$), at which a sample is assigned to the electric poling until an ending temperature ($T_{end} \sim 2$ K in the lowest limit of the present experimental environment). In our experiments, the same sample may show qualitatively different data of $I(T)$ and $P(T)$ if T_{st} is different. This effect has rarely been observed before and the results imply that the low-T multiferroicity can be controlled by assigning different polarized states in the high-T range.

In fact, it was reported in 2015 that the lattice structure of RMn$_2$O$_5$ family at ambient temperature may belong to the non-centrosymmetric Pm space group rather than the centrosymmetric $Pbam$.[36] This work has caught attention in the past three years,[35,37–45] and some doubtable ferroelectric loops in the high-T range were measured.[46,47] While this dispute has not been settled, the possibility of polar lattice structure in the high-T range may allow an opportunity to correlate the data scattering of the low-T multiferroicity with the high-T polarized state induced by electric poling or other stimuli. Here, it might be delicate to claim the high-T state as a "polarized state" since the polar Pm lattice structure is questionable and the physical mechanism is pendent. In this paper, the terminology of "polarized state" refers to an electrically poled state in a narrow sense, though nearly no ferroelectricity in the high-T range for most of RMn$_2$O$_5$ members has not yet been confirmed mainly due to the leaky problem. If this is true, the measured $I(T)$ data below T_{N1} by using the pyroelectric method could depend on the magnetically induced component and high-T polarized state. Possible contributions from local lattice/nuclear or other degrees of freedom might be frozen at low T and the memory of the specific high-T configuration is kept. These issues thus arouse substantial interest in investigating the low-T multiferroicity of RMn$_2$O$_5$ for different high-T poling sequences.

Since the specific constraints producing the low-T configuration are not exactly known, tackling the electrical degree of freedom over T in spite of other degrees of freedom at fixed T could be of great help. In this work, we intend to deal with this issue and take GdMn$_2$O$_5$ as our object. The GdMn$_2$O$_5$ was reported to have the largest polarization in the absence of magnetic field, and a magnetic field of 2.0 T can flip the low-T polarization, inducing a big change ($\Delta P = 5000$ μC/m^2).[30] However, no such flip by a magnetic field up to $\mu_0 H = 9$ T was observed in another report, making the underlying physics puzzling.[31] In addition, the low-T magnetic ordering of this system with only two magnetic transitions at T_{N1} and T_{N2} associated with the Mn spin ordering has been identified. The Gd spin is roughly isotropic and its independent ordering occurs only at very low T (at T_{Gd}). This implies that the Gd spin may be aligned with the neighboring Mn spin but it can be easily re-aligned by an external field (such as a weak magnetic field).[48] Moreover, it is found that the magnetoelectric effect at $T \ll T_{N2}$ is remarkable, while the polarization around T_{N2} is almost insensitive to magnetic field.[31,49] As a result, GdMn$_2$O$_5$ seems to be an example to explore the possible correlation between the low-T multiferroicity and the high-T polarized state. Polycrystalline samples are chosen for some reasons, which will be discussed in Supplementary Material.

2. Experimental details

The single-phase polycrystalline GdMn$_2$O$_5$ was prepared by the conventional solid-state reaction method. The highly purified powder of Gd$_2$O$_3$ and Mn$_2$O$_3$ were mixed in stoichiometric ratio, ground, and then fired at 1200 °C for 24 h in a

flowing oxygen atmosphere. The resulting powder was fully re-ground and pelletized under 70 MPa pressure into disks of 2 cm in diameter, and then the pellets were sintered at 1400 °C for 24 h in a flowing oxygen sphere prior to cooling down naturally to room temperature. The sample crystallinity and structure were checked by x-ray diffraction (XRD) with CuKα radiation at room temperature. The refinement of XRD data was performed by using the standard Rietveld method. The chemical composition and its spatial homogeneity on a nanoscale were probed using scanning electron microscopy (SEM, Hitachi S-4800) to ascertain the microstructure.

For the electrical measurements, Au electrodes were deposited on either side of each of the disk-like samples of 3.0 mm in diameter and 0.2 mm in thickness. The electric polarization P as a function of T in the low-T range ($< T_{N1}$) was evaluated from the pyroelectric current $I(T)$ data. It should be noted that this polarization is relatively small so that conventional method such as positive-up negative-down method cannot give sufficiently reliable results.

In order to investigate the influence of the high-T polarized state on the low-T multiferroic behavior, we designed a set of specific experiments, which will be described in detail in Section 3. For the common pyroelectric measurements, an electric poling was applied to each sample by an electric source with a compliance current of ~ 0.1 mA. The applied voltage was 200 V for the sample of 0.02 cm in thickness, corresponding to a poling field of 10 kV/cm. Hereafter, the poling electric field is denoted as E_p. By this scheme, the sample was cooled down from a given temperature T_{st} (to room temperature) to an final temperature T_{end} (down to 2 K). Then the sample was electrically short-circuited for sufficient time (in our work, the short-circuit time was set to be about 60 min to reduce the background current) at T_{end}, followed by a slow heating up to a temperature higher than T_{N1}, during which the electric current released from the capacitor was recorded by using the Keithley 6514 A electrometer. The heating rate v_t may be varied from 2.0 K/min to 6.0 K/min in different measuring cycles. The polarization P was then calculated by integrating the pyroelectric current $I(T)$.

Here it should be mentioned that the collection of $I(T)$ data was terminated at $T = 60$ K, and no more data above this temperature would be provided. For all the cases, the current between T_{N1} and $T = 60$ K was zero within the measuring uncertainties. Therefore, the evaluated $P(T)$ here only contained the magnetism-induced polarization, but no contribution from the high-T polarized state, if any. It should also be mentioned that the probed current in the present measurements did not contain any leaky signals since no electric bias had been applied to the sample. The possible other contributions may be from the trapped charges in the shallow levels which are de-trapped during the sample heating.[50] This contribution, if any, can be extracted by comparing the $I(T)$ curves measured at different heating rates.

3. Results and discussion

3.1. Microstructures and low-T multiferroicity

The characterizations of microstructures and chemical homogeneity of the samples are performed by measuring the XRD θ–2θ spectra and SEM observation. All the XRD peaks can be properly indexed by the standard reflections without identifiable impurity phase as presented in Fig. 1(b). For simplicity, we still adopt the centrosymmetric *Pbam* space group to index the spectra. Rietveld refinement is adopted to fit the measured XRD data, and good agreement is obtained with $R_{wp} = 6.12\%$, $R_p = 4.85\%$, and $\chi^2 = 1.069$. The refined lattice parameters are $a = 7.332$ Å, $b = 8.508$ Å, and $c = 5.662$ Å, which are well consistent with earlier reported results.[51] The microstructures and homogeneous planar spatial distributions of Gd and Mn are shown in Fig. S2. The densely packed grains show an average size of ~ 1.0 μm, excluding safely the surface self-polarized effect.

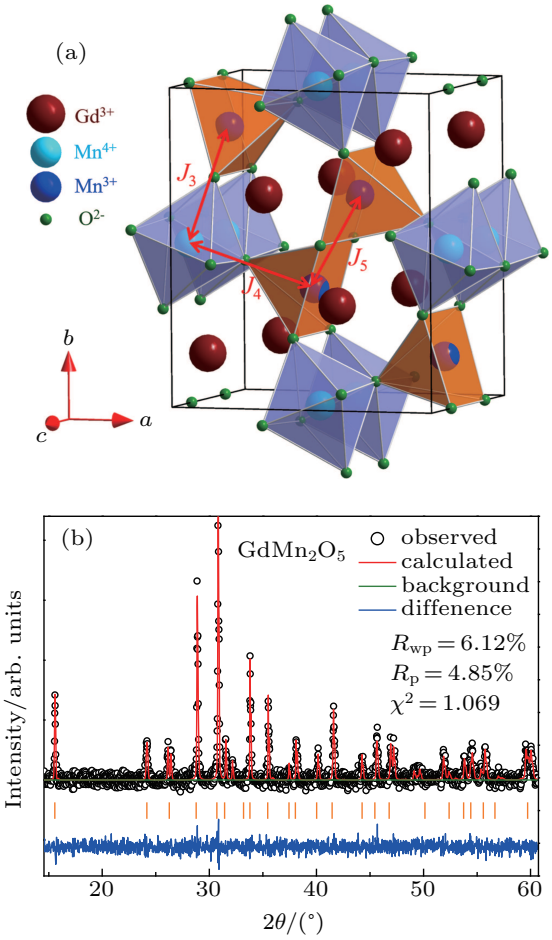


Fig. 1. (a) Schematic drawing of the lattice structure of $GdMn_2O_5$ with three major Mn–Mn exchanges J_3, J_4, and J_5; (b) measured θ–2θ XRD spectrum of polycrystalline sample and Rietveld method refined data for comparison.

For more data about the specific heat, lattice distortion, and magnetism, one may refer to earlier work on RMn_2O_5,[19,24,26,52] as well as our characterization in Fig. S3

of Supplementary Material. Here these results are briefly summarized as follows. First, three anomalies are observed respectively at temperatures $T_{N1} \sim 41.0$ K, $T_{N2} \sim 33.0$ K, and $T_{Gd} \sim 3.5$ K, which indicate the multiferroic/magnetic phase transitions. Second, around T_{Gd}, a weak but clear peak appears, manifesting a ferroelectric transition associated with the independent Gd^{3+} spin–ordering, which is different from the reported behavior for single crystal sample.[30] All of these are the typical features of type-II multiferroics. Moreover, we check the reliability of the pyroelectric method in our measurements as shown in Fig. S4. The under-curve area of measured $I(T)$ is roughly proportional to the heating rate, revealing that the measured current signals have no contribution from the detrapped charges during the sample heating, *i.e.*, the charges come entirely from the pyroelectric effect.

3.2. Low-T ferroelectricity associated with high-T polarized states

According to the above results of the low-T multiferroic properties, one can now measure the variations of these properties in response to different high-T polarized states. We first perform extensive measurements and then refine several representative sequences for the present study as schematically shown in Fig. 2. Here, the arrow indicates the poling path. Starting from $T_{st} = 300$ K, a direct current (DC) electric field E_{p1} is applied to the sample during gradually cooling down to a "switching temperature", T_{sw}, and then the field is switched to another value E_{p2} until T_{end}. It is noted that E_{p1} and E_{p2} can be positive or negative. For convenience, each case shown in Fig. 2 is abbreviated as Eab $(a, b = +, -, 0)$. For example, $E+-$ indicates $E_{p2} > 0$ and $E_{p1} < 0$ while $E+0$ refers to $E_{p2} > 0$ and $E_{p1} = 0$. We only consider the data measured under the poling field $E_p = \pm 10$ kV/cm and 0. In our following experiments, we set $v_t = 2$ K/min, $T_{sw} = 45$ K (slightly higher than T_{N1}), and $T_{end} = 2$ K, unless otherwise stated.

We present in Fig. 3 the measured $I(T)$ curves and evaluated $P(T)$ curves under eight different poling sequences ($E0\pm$, $E\pm0$, $E+-$, $E--$, $E++$, and $E--$ modes), respectively. It comes immediately to us that the low-T ferroelectricity is tightly correlated with the high-T polarized state. For nonzero E_{p1} and zero E_{p2} ($E0\pm$), one can still detect remarkable signals $I(T)$ and $P(T)$. Surprisingly, the positive E_{p1} induces a sharp $I(T)$ valley around T_{N2} and a negative P below T_{N2}, while the negative E_{p1} generates a positive P below T_{N2} as shown in Figs. 3(a) and 3(b). For zero E_{p1} and nonzero E_{p2} ($E\pm0$) shown in Figs. 3(c) and 3(d), we observe the pyroelectric current $I(T)$ that has been discussed in Fig. S3(c) before. The current is always positive or negative in the whole T-range below T_{N2}, depending on the nonzero poling field E_{p2} that appears in the temperature range from T_{sw} to T_{end}. Moreover, the $I(T)$ curve for $E_{p1} < 0$ and $E_{p2} > 0$ ($E+-$ case) exhibits a much higher peak around T_{N2}, and the current peak shifts slightly toward the high-T side. Again, these data are surprising since a negative E_{p1} applied to the sample here does influence the polarization, while it is believed to be paraelectric when $T > T_{sw} > T_{N2}$. This is certainly in discrepancy with conventional ferroelectric scenario. The data in the $E-+$ case reveal the same feature. On the other hand, looking at the $I(T)$ curve for $E_{p1} > 0$ and $E_{p2} > 0$ ($E++$ case), it is even more surprising that the current peak around T_{N2} becomes negative and then switches to a positive value around 30 K. The data in the $E--$ case also reveal the same feature. For all these cases, the current profiles around T_{Gd} remain roughly similar except for a weak anomaly at T_{Gd}.

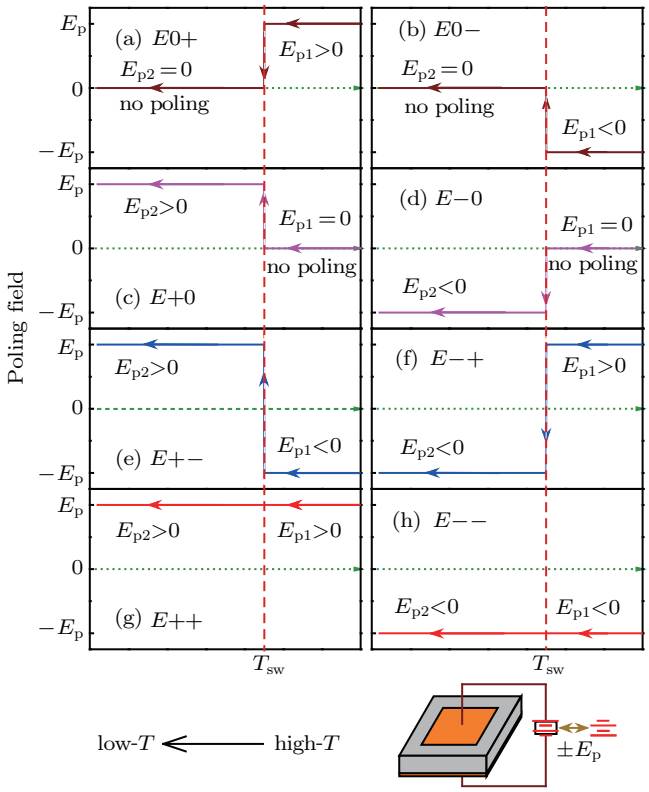


Fig. 2. (a)–(h) Electric poling sequences designed for the present experiments: modes $E0+$, $E0-$, $E+0$, $E-0$, $E+-$, $E-+$, $E++$, and $E--$, respectively. Here, field E_{p1} is applied in the temperature range from $T_{st} = 300$ K to $T_{sw} = 45$ K, and field E_{p2} is applied from $T_{sw} = 45$ K to $T_{end} = 2$ K. The corresponding device is schematically drawn below.

It is clearly demonstrated from the evaluated $P(T)$ data in Fig. 3 that the high-T polarized state plays a major role in the low-T ferroelectricity. First, the curves at $E+-$ and $E-+$ are symmetric with respect to each other, so are the curves at $E+0$ and $E-0$, the curves at $E0+$ and $E0-$, and the curves at $E++$ and $E--$. Second, the sign of polarization at the emerging point T_{N2} seems to be determined by the sign of the poling field E_{p1}, suggesting that more than one polarization component exists in $GdMn_2O_5$, and at least one of them is correlated to E_{p1}. Third, we look at the signs of polarizations around T_{N2} and T_{Gd}, $P(T_{N2})$ and $P(T_{Gd})$, respectively, and the dependence of the sign on E_{p1} and E_{p2} is summarized in Table 1. In short, the sign of $P(T_{N2})$ is opposite to that of E_{p1} and the sign of $P(T_{Gd})$ is the same as that of E_{p2}.

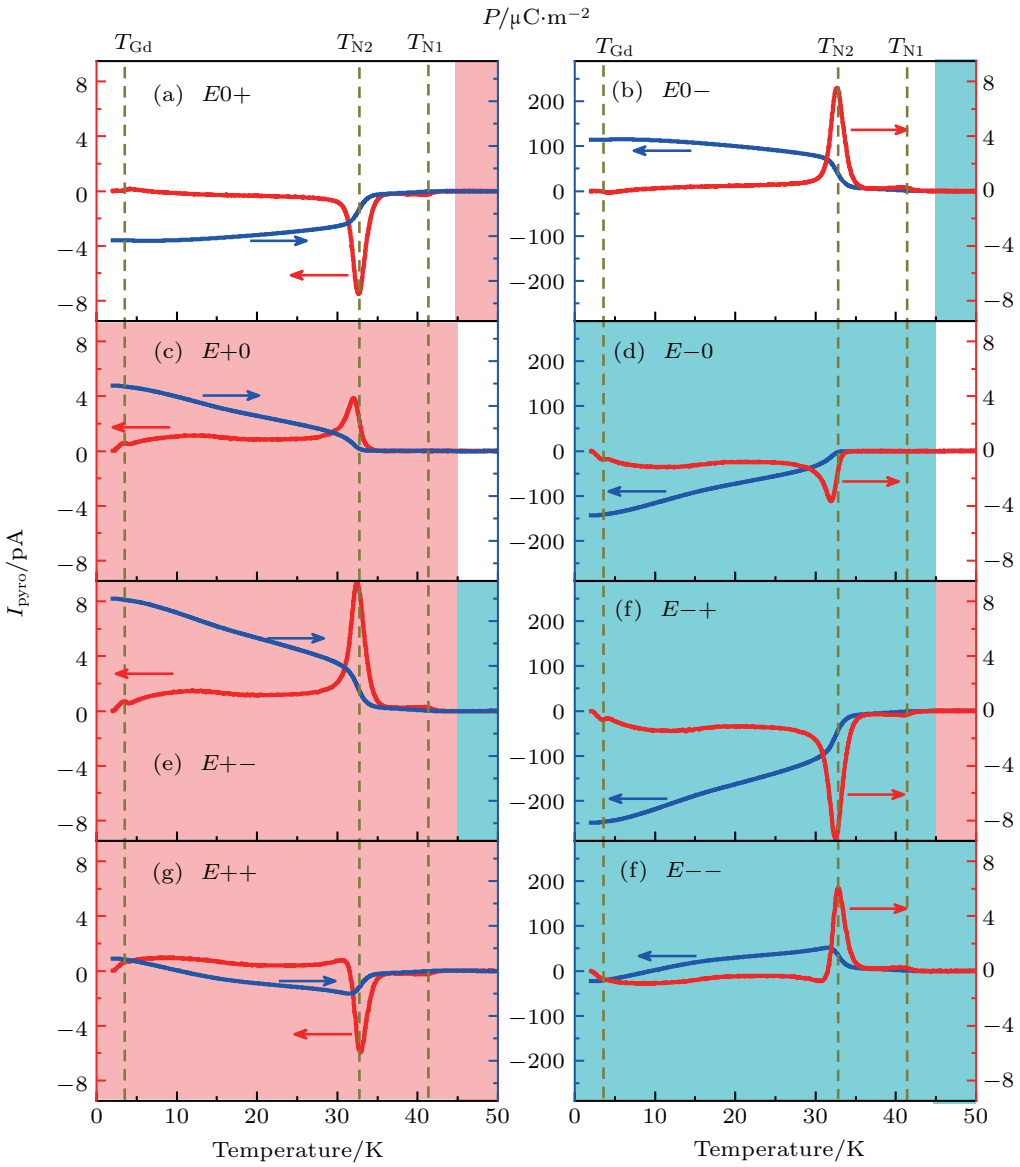


Fig. 3. ((a)–(h)) Measured $I(T)$ curves (red) and evaluated $P(T)$ curves (blue) in eight poling modes $E0+$, $E0-$, $E+0$, $E-0$, $E+-$, $E++$, and $E--$, respectively. Characteristic temperatures T_{N1}, T_{N2}, and T_{Gd} are marked. Colored blocks represent applied poling fields in corresponding regions during sample cooling, with pink denoting E_p, cyan denoting $-E_p$, and white denoting 0.

Table 1. Signs of several polarizations and their dependence on sign of E_{p1} and E_{p2}.

quantity sign	E_{p1}		E_{p2}	
	+	−	+	−
P_{MM}	−	+		
P_{GM}			+	−
$P(T_{N2})$	−	+		
$P(T_{Gd})$			+	−

3.3. Two polarization components

As stated above, obviously, there should exist more than one polarization component in the low-T range ($T < T_{sw}$), and here we only consider two components for simplicity. One component is P_{MM} that emerges around T_{N2}. This component seems to be controlled by poling field E_{p1}, and the sign of P_{MM} is opposite to that of E_{p1}. The other component is P_{GM} that also emerges around T_{N2}, but the emerging point is slightly lower than that for P_{MM}. This component seems to be controlled by poling field E_{p2}, and its sign is the same as that of E_{p2}. The total polarization P_{tot} would be the sum of the two components, *i.e.*, $P_{tot} = P_{MM} + P_{GM}$.

To further confirm the existence of component P_{MM}, we look again at the $I(T)$ data for two specific poling sequences: $E0-$ and $E0+$, while the data at $E00$ are probed as a reference. The data are plotted in Fig. 4(a). While no remarkable signal is detected for the case of $E00$, positive $I(T)$ and negative $I(T)$ with corresponding peaks around T_{N2} are recorded respectively. Moreover, to confirm the existence of component P_{GM}, we also plot the $I(T)$ data for two other specific sequences: $E+0$ and $E-0$ in Fig. 4(a). Clearly, the positive and negative $I(T)$ with corresponding peaks around T_{N2} are probed, confirming that the component P_{GM} is essentially aligned by the poling field E_{p2}.

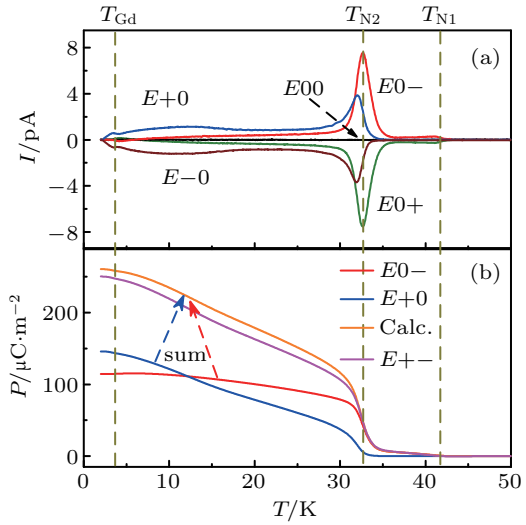


Fig. 4. (a) Measured $I(T)$ curves in $E0-$, $E0+$, $E+0$, $E-0$, and $E00$ modes, and (b) Evaluated $P(T)$ curves in $E0-$, $E+0$, $E+-$ modes with the calculated polarization $P_{calc} = P(E0-) + P(E+0)$, showing that P_{calc} is well consistent with total polarization in $E+-$ mode.

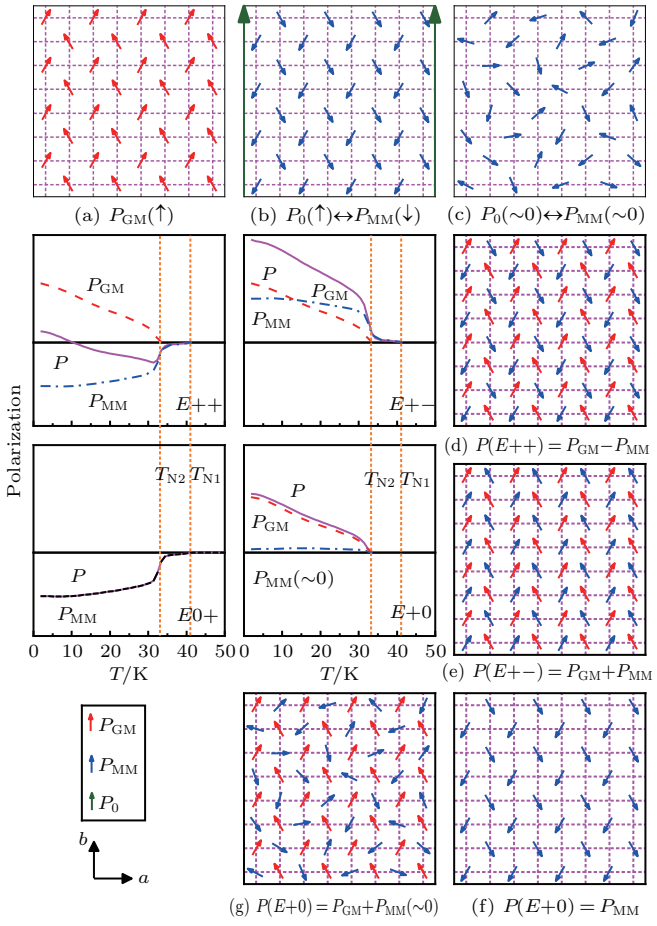


Fig. 5. Proposed microscopic mechanisms for polarization components P_{MM} and P_{GM} and their responses to four chosen electric poling modes: $E++$, $E+-$, $E0+$, and $E+0$ respectively. Total polarization $P_{tot} = P_{MM} + P_{GM}$. Here P_0 is assumed to be polarization of the high-T polarized state. Two components P_{MM} and P_{GM} constitute respectively a sublattice as shown in panels (a) and (b). P_{MM} is clamped by high-T polarized state in the antiparallel form ($P_{MM} \uparrow\downarrow$ "P_0") but P_{GM} is aligned by E_{p2} applied below T_{sw}. $P_{MM} \sim 0$ if "P_0" ~ 0, *i.e.*, $E_{p1} = 0$ as shown in panel (c). The low-T polarization lattices for the four modes are plotted in panels (d), (e), (f), and (g), respectively.

For this stage, a crude and probably over-simplified assumption can be made: it is noted that the two components P_{MM} and P_{GM} are mainly aligned by poling fields E_{p1} and E_{p2} respectively, while at the same time they are most likely irrelevant with the other one (poling field). It is interesting to note that the obtained $P_{tot}(T)$ curve by summing $P_{MM}(T)$ curve under poling $E0-$ and $P_{GM}(T)$ curve under poling $E+0$ is well consistent with the measured $P(T)$ curve under poling $E+-$ as shown in Fig. 4(b). This consistency further confirms the above assumption, which allows us to discuss all the measured $P(T)$ data under various poling sequences based on this assumption. For convenience of illustration, we present in Fig. 5 the measured $P(T)$ curves under the poling sequences $E++$, $E+-$, $E0+$, $E+0$. It is seen that all the curves can be well described by the different combinations of the two components, indicating that the low-T ferroelectricity below T_{N1} for $GdMn_2O_5$ is indeed a property of two-component physics.

Certainly, the two polarization components are magnetism-related. As suggested earlier, component P_{MM} can be assigned to the Mn–Mn symmetric exchange striction induced polarization and component P_{GM} to the Gd–Mn symmetric exchange striction induced component. For $GdMn_2O_5$, it seems that the two components are not coupled with each other as in the case of $DyMn_2O_5$. This is understandable since the Gd spins were reported to be somehow isotropic and not tightly clamped by the neighboring Mn spins.[30,48] Although the ground state favors the parallel/antiparallel alignment of Gd spins with the neighboring Mn spins, the electric poling by E_{p2} below T_{sw} may induce the Gd spins to flip from one direction to its opposite direction due to the flip of P_{GM}.

3.4. Clamping of P_{MM} by high-T polarized state

The core phenomenon observed in the present experiments is that component P_{MM} is always opposite to poling field E_{p1} that is applied in the high-T range but terminated at a temperature T_{sw} slightly higher than T_{N1}. This is also one of the core issues for understanding the low-T multiferroicity of $GdMn_2O_5$, or even the other members in the same family. This puzzling phenomenon raises serious concerns about the high-T polarized state that may determine the orientation of P_{MM}. Since P_{MM} is magnetism-generated and it will not appear until $T_{N2} < T_{N1} < T_{sw}$, the high-T magnetic fluctuations above T_{N1}, if any, may influence the magnitude of P_{MM} by reconfiguring the Mn spin ordering but have no way to determine the direction of P_{MM}. The only possibility here is that there exists a high-T polarized state with a "virtual polarization P_0", if this state is electrically aligned by poling field E_{p1}. This "P_0" is well saturated in the low-T range and thus contributes no pyroelectric current in the whole T-range below T_{sw}.

Given this well-aligned high-T polarized state with "P_0" parallel to E_{p1}, the observed puzzling effect may be explained qualitatively. This polarized state is aligned by E_{p1} from

$T_{st} = 300$ K until $T_{sw} = 45$ K that is sufficiently low for freezing this state. In this case, no matter whether a positive or negative E_{p1} enters below T_{sw}, this polarized state remains well frozen without much change until T_{end}. Our measured results suggest that this well-aligned polarized state does clamp the subsequently-appearing magnetism-induced polarization P_{MM} at T_{N2}, i.e. P_{MM} is always antiparallel to "P_0", or E_{p1}.

The antiparallel clamping of P_{MM} by "P_0" is only a crude hypothesis without sufficient evidence so far. It is just proposed here to explain the observed results. Even so, one still has several reasons to favor this hypothesis. First, based on this hypothesis, the measured results about the low-T ferroelectricity can be reasonably understood. Second, earlier first-principles calculations on $HoMn_2O_5$ did reveal the existence of two polarization components: ionic polarization and electronic polarization, and they are antiparallel to each other.[53] Neither of the two polarizations related to the Mn ions' contributions, corresponds to the "P_0" or P_{MM} here, but it is inferred that the two polarizations are usually antiparallel if they coexist simultaneously in a system in order to lower the electrostatic energy. Third, one may discuss a specific case for the poling sequence $E + 0$ or $E - 0$. If no such clamping effect between P_{MM} and "P_0" exists, poling field E_{p2} applied in a temperature range from $T_{sw} > T_{N2}$ to T_{end} would align both P_{MM} and P_{GM} in the same direction, leading to a large P_{tot}. However, our measured polarization is only P_{GM} as shown in Fig. 3. This suggests "P_0" = 0 if $E_{p1} = 0$ and thus $P_{MM} \sim 0$, i.e., the local P_{MM} is always clamped by the local "P_0".

3.5. Discussion

All of our discussion on the measured results of $GdMn_2O_5$ reveals two major facts. On the one hand, it is revealed that the possible high-T polarized state has a strong influence on the low-T multiferroic behavior, in particular, the low-T ferroelectric polarization. Certainly, the Mn spin configuration would be dependent on the high-T polarized state although this prediction needs direct evidence from magnetic structure probing. This influence allows the low-T multiferroicity to be tuned by the high-T electric poling, which represents an electric control of multiferroicity or magnetism in the specific sense. On the other hand, it is claimed that the high-T polarized state can clamp the magnetism-induced polarization P_{MM} below T_{N2}, making the low-T multiferroicity fascinating. These two facts allow us to map the electric control of the low-T ferroelectricity for the four typical different poling sequences, referring to the proposed mechanisms for generating the two polarization components via the Mn–Mn and Gd–Mn symmetric exchange strictions.[33] The corresponding spin structures at low T are schematically drawn for illustration in Fig. 5, using the main results revealed in the present work.

Nevertheless, the deficiencies or issues, requiring future investigation are also obvious. First, insufficient evidence for the high-T polarized state, or more specifically, no nature of this polarized state is given in the present work. It is a big challenge to probe the polarized state in the high-T range due to the very leaky problem, and more, whether this state is true is still a question. This problem is essential due to the narrow bandgap of RMn_2O_5. Second, it is observed that polarization components P_{MM} and P_{GM} are non-coupled or only loosely coupled. The underlying physics remains to be revealed by carefully determining the Gd and Mn spin structures in the low-T range, such as by using neutron scattering. Third, we come back to the issue of sample quality. The careful and reliable measurements on single crystals rather than polycrystalline samples would be highly preferred for additionally validating the conclusion of this work, although an effective approach to excluding the strong self-polarized effect on the single crystal surfaces would be a big challenge.

4. Conclusions

In the present work, focusing on the correlation of the probable high-T polarized state with the magnetically induced electric polarization in the low-T range, we perform extended measurements of $GdMn_2O_5$ in its polycrystalline form. It is revealed that the high-T electric poling routine plays a vital role in controlling the low-T multiferroic behavior. The results suggest that there are two main magnetism-related polarization components responsible for the observed unique scenarios, which refer to component P_{MM} generated by the Mn–Mn exchange striction and component P_{GM} generated by the Gd–Mn exchange striction. The component P_{MM} is obviously tightly clamped by the high-T polarized state while the component P_{GM} is not. The present work provides a comprehensive understanding of the relationship between low-T multiferroicity and high-T polarized state in $GdMn_2O_5$, and also presents a representative case where how multiferroicity can be controlled by electrical poling.

References

[1] Kimura T, Goto T, Shintani H, Ishizaka K, Arima T and Tokura Y 2003 *Nature* **426** 55
[2] Khomskii D 2009 *Physics* **2** 20
[3] Dong S, Yu R, Yunoki S, Liu J M and Dagotto E 2008 *Phys. Rev. B* **78** 155121
[4] Katsura H, Nagaosa N and Balatsky A V 2005 *Phys. Rev. Lett.* **95** 057205
[5] Jia C, Onoda S, Nagaosa N and Han J H 2006 *Phys. Rev. B* **74** 224444
[6] Mochizuki M, Furukawa N and Nagaosa N 2011 *Phys. Rev. B* **84** 144409
[7] Fiebig M 2005 *J. Phys. D: Appl. Phys.* **38** R123
[8] Wang K F, Liu J M and Ren Z F 2009 *Adv. Phys.* **58** 321
[9] Kimura T 2007 *Ann. Rev. Mater. Res.* **37** 387
[10] Xu K, Lu X Z and Xiang H 2017 *Npj Quantum Mater.* **2** 1
[11] Zhang G, Dong S, Yan Z, Guo Y, Zhang Q, Yunoki S, Dagotto E and Liu J M 2011 *Phys. Rev. B* **84** 174413

[12] Johnson R D, Chapon L C, Khalyavin D D, Manuel P, Radaelli P G and Martin C 2012 *Phys. Rev. Lett.* **108** 067201
[13] Caignaert V, Maignan A, Singh K, Simon C, Pralong V, Raveau B, Mitchell J F, Zheng H, Huq A and Chapon L C 2013 *Phys. Rev. B* **88** 174403
[14] Zhou L, Wang X, Zhang X M, Shen X D, Dong S and Long Y W 2018 *Acta Phys. Sin.* **67** 157505 (in Chinese)
[15] Ratcliff W, Lynn J W, Kiryukhin V, Jain P and Fitzsimmons M R 2016 *Npj Quantum Mater.* **1** 16003
[16] Lu C and Liu J M 2016 *J. Materiomics* **2** 213
[17] Pang H, Zhang F, Zeng M, Gao X, Qin M, Lu X, Gao J, Dai J and Li Q 2016 *Npj Quantum Mater.* **1** 16015
[18] Higashiyama D, Miyasaka S and Tokura Y 2005 *Phys. Rev. B* **72** 064421
[19] Tachibana M, Akiyama K, Kawaji H and Atake T 2005 *Phys. Rev. B* **72** 224425
[20] Fukunaga M, Sakamoto Y, Kimura H, Noda Y, Abe N, Taniguchi K, Arima T, Wakimoto S, Takeda M, Kakurai K and Kohn K 2009 *Phys. Rev. Lett.* **103** 077204
[21] Blake G R, Chapon L C, Radaelli P G, Park S, Hur N, Cheong S W and Rodríguez-Carvajal J 2005 *Phys. Rev. B* **71** 214402
[22] Radaelli P G and Chapon L C 2008 *J. Phys.: Condens. Matter* **20** 434213
[23] Chapon L C, Blake G R, Gutmann M J, Park S, Hur N, Radaelli P G and Cheong S W 2004 *Phys. Rev. Lett.* **93** 177402
[24] dela Cruz C R, Yen F, Lorenz B, Gospodinov M M, Chu C W, Ratcliff W, Lynn J W, Park S and Cheong S W 2006 *Phys. Rev. B* **73** 100406
[25] Ratcliff W, Kiryukhin V, Kenzelmann M, Lee S H, Erwin R, Schefer J, Hur N, Park S and Cheong S W 2005 *Phys. Rev. B* **72** 060407
[26] Noda Y, Kimura H, Fukunaga M, Kobayashi S, Kagomiya I and Kohn K 2008 *J. Phys.: Condens. Matter* **20** 434206
[27] Lu C L, Fan J, Liu H M, Xia K, Wang K F, Wang P W, He Q Y, Yu D P and Liu J M 2009 *Appl. Phys. A* **96** 991
[28] Zhao Z Y, Liu M F, Li X, Lin L, Yan Z B, Dong S and Liu J M 2015 *Sci. Rep.* **4** 3984
[29] Bukhari S H and Ahmad J 2017 *Chin. Phys. B.* **26** 018103
[30] Lee N, Vecchini C, Choi Y J, Chapon L C, Bombardi A, Radaelli P G and Cheong S W 2013 *Phys. Rev. Lett.* **110** 137203
[31] Bukhari S H, Kain T, Schiebl M, Shuvaev A, Pimenov A, Kuzmenko A M, Wang X, Cheong S W, Ahmad J and Pimenov A 2016 *Phys. Rev. B* **94** 174446
[32] Kato S, Kohn K and Ishikawa M 1997 *Ferroelectrics* **203** 323
[33] Liu J M and Dong S 2015 *J. Adv. Dielect.* **05** 1530003
[34] Zhao Z Y, Liu M F, Li X, Wang J X, Yan Z B, Wang K F and Liu J M 2014 *J. Appl. Phys.* **116** 054104
[35] Yang L, Li X, Liu M F, Li P L, Yan Z B, Zeng M, Qin M H, Gao X S and Liu J M 2016 *Sci. Rep.* **6** 34767
[36] Balédent V, Chattopadhyay S, Fertey P, Lepetit M B, Greenblatt M, Wanklyn B, Saouma F O, Jang J I and Foury-Leylekian P 2015 *Phys. Rev. Lett.* **114** 117601
[37] Basu T, Singh K, Gohil S, Ghosh S and Sampathkumaran E V 2015 *J. Appl. Phys.* **118** 234103
[38] Deutsch M, Hansen T C, Fernandez-Diaz M T, Forget A, Colson D, Porcher F and Mirebeau I 2015 *Phys. Rev. B* **92** 060410
[39] Chattopadhyay S, Balédent V, Damay F, Gukasov A, Moshopoulou E, Auban-Senzier P, Pasquier C, André G, Porcher F, Elkaim E, Doubrovsky C, Greenblatt M and Foury-Leylekian P 2016 *Phys. Rev. B* **93** 104406
[40] Mansouri S, Jandl S, Balli M, Laverdière J, Fournier P and Dimitrov D Z 2016 *Phys. Rev. B* **94** 115109
[41] Moshopoulou E G, Foury-Leylekian P, Page K, Doubrovsky C, Greenblatt M and Hurd A J 2016 *Nanoscale Ferroelectrics and Multiferroics* (John Wiley & Sons, Ltd) pp. 375–399
[42] Vorob'ev S I, Andrievskii D S, Barsov S G, Getalov A L, Golovenchits E I, Komarov E N, Kotov S A, Mishchenko A Y, Sanina V A and Shcherbakov G V 2016 *J. Exp. Theor. Phys.* **123** 1017
[43] Ahmad J, Bukhari S H, Jamil M T, Rehmani M K, Ahmad H and Sultan T 2017 *Adv. Condens. Matter Phys.* **2017** 5389573
[44] Tung Y H, Yang C C, Hsu T W, Kao C W and Chen Y Y 2017 *AIP Adv.* **7** 055830
[45] Yahia G, Damay F, Chattopadhyay S, Balédent V, Peng W, Elkaim E, Whitaker M, Greenblatt M, Lepetit M B and Foury-Leylekian P 2017 *Phys. Rev. B* **95** 184112
[46] Khannanov B K, Sanina V A, Golovenchits E I and Scheglov M P 2016 *JETP Lett.* **103** 248
[47] Khannanov B K, Sanina V A, Golovenchits E I and Scheglov M P 2017 *J. Magn. Magn. Mater.* **421** 326
[48] Vecchini C, Bombardi A, Chapon L C, Lee N, Radaelli P G and Cheong S W 2014 *J. Phys: Conf. Ser.* **519** 012004
[49] Popov Y F, Kadomtseva A M, Vorob'ev G P, Krotov S S, Kamilov K I and Lukina M M 2003 *Phys. Solid State* **45** 2155
[50] Ngo T N M, Adem U and Palstra T T M 2015 *Appl. Phys. Lett.* **106** 152904
[51] Satoh H, Suzuki S, Yamamoto K and Kamegashira N 1996 *J. Alloys Compd.* **234** 1
[52] Kimura H, Kobayashi S, Wakimoto S, Noda Y and Kohn K 2007 *Ferroelectrics* **354** 77
[53] Giovannetti G and van den Brink J 2008 *Phys. Rev. Lett.* **100** 227603